

Fast Variability of Tera–Electron Volt γ Rays from the Radio Galaxy M87

F. Aharonian,¹ A. G. Akhperjanian,² A. R. Bazer-Bachi,³ M. Beilicke,^{4*} W. Benbow,¹ D. Berge,¹ K. Bernlöhr,^{1,5} C. Boisson,⁶ O. Bolz,¹ V. Borrel,³ I. Braun,¹ A. M. Brown,⁷ R. Bühler,¹ I. Büsching,⁸ S. Carrigan,¹ P. M. Chadwick,⁷ L.-M. Chouet,⁹ G. Coignet,¹⁰ R. Cornils,⁴ L. Costamante,^{1,23} B. Degrange,⁹ H. J. Dickinson,⁷ A. Djannati-Atai,¹¹ L. O’C. Drury,¹² G. Dubus,⁹ K. Egberts,¹ D. Emmanoulopoulos,¹³ P. Espigat,¹¹ F. Feinstein,¹⁴ E. Ferrero,¹³ A. Fiasson,¹⁴ G. Fontaine,⁹ Seb. Funk,⁵ S. Funk,¹ M. Füßling,⁵ Y. A. Gallant,¹⁴ B. Giebels,⁹ J. F. Glicenstein,¹⁵ P. Goret,¹⁵ C. Hadjichristidis,⁷ D. Hauser,¹ M. Hauser,¹³ G. Heinzlmann,⁴ G. Henri,¹⁶ G. Hermann,¹ J. A. Hinton,^{1,13} A. Hoffmann,¹⁷ W. Hofmann,¹ M. Holleran,⁸ S. Hoppe,¹ D. Horns,¹⁷ A. Jacholkowska,¹⁴ O. C. de Jager,⁸ E. Kendziorra,¹⁷ M. Kerschhaggl,⁵ B. Khélifi,^{9,1} Nu. Komin,¹⁴ A. Konopelko,^{5†} K. Kosack,¹ G. Lamanna,¹⁰ I. J. Latham,⁷ R. Le Gallou,⁷ A. Lemièrè,¹¹ M. Lemoine-Goumard,⁹ J.-P. Lenain,⁶ T. Lohse,⁵ J. M. Martin,⁶ O. Martineau-Huynh,¹⁸ A. Marcowith,³ C. Masterson,^{1,23} G. Maurin,¹¹ T. J. L. McComb,⁷ E. Moulin,¹⁴ M. de Naurois,¹⁸ D. Nedbal,¹⁹ S. J. Nolan,⁷ A. Noutsos,⁷ K. J. Orford,⁷ J. L. Osborne,⁷ M. Ouchrif,^{18,23} M. Panter,¹ G. Pelletier,¹⁶ S. Pita,¹¹ G. Pühlhofer,¹³ M. Punch,¹¹ S. Rançon,¹⁰ B. C. Raubenheimer,⁸ M. Raue,⁴ S. M. Rayner,⁷ A. Reimer,²⁰ J. Ripken,⁴ L. Rob,¹⁹ L. Rolland,¹⁵ S. Rosier-Lees,¹⁰ G. Rowell,¹ V. Sahakian,² A. Santangelo,¹⁷ L. Saugé,¹⁶ S. Schlenker,⁵ R. Schlickeiser,²⁰ R. Schröder,²⁰ U. Schwanke,⁵ S. Schwarzburg,¹⁷ S. Schwemmer,¹³ A. Shalchi,²⁰ H. Sol,⁶ D. Spangler,⁷ F. Spanier,²⁰ R. Steenkamp,²¹ C. Stegmann,²² G. Superina,⁹ P. H. Tam,¹³ J.-P. Tavernet,¹⁸ R. Terrier,¹¹ M. Tluczykont,^{9,23} C. van Eldik,¹ G. Vasileiadis,¹⁴ C. Venter,⁸ J. P. Vialle,¹⁰ P. Vincent,¹⁸ H. J. Völk,¹ S. J. Wagner,¹³ M. Ward⁷

The detection of fast variations of the tera–electron volt (TeV) (10^{12} eV) γ -ray flux, on time scales of days, from the nearby radio galaxy M87 is reported. These variations are about 10 times as fast as those observed in any other wave band and imply a very compact emission region with a dimension similar to the Schwarzschild radius of the central black hole. We thus can exclude several other sites and processes of the γ -ray production. The observations confirm that TeV γ rays are emitted by extragalactic sources other than blazars, where jets are not relativistically beamed toward the observer.

So far, the only extragalactic objects known to emit γ radiation up to energies of Tera electron volts (1 TeV = 10^{12} eV) are blazars. These are active galactic nuclei (AGN) with a plasma jet emanating from the vicinity of the black hole and pointing close to the observer’s line of sight. Because of the bulk relativistic motion of the plasma in the jet, the energy and luminosity of emitted photons are boosted by relativistic effects, making blazars detectable up to TeV energies.

The nearby radio galaxy M87 is located in the Virgo cluster of galaxies at a distance of ~ 16 Mpc ($z = 0.0043$) and hosts a central black hole of $(3.2 \pm 0.9) \times 10^9$ solar masses (1). The 2-kpc scale plasma jet (2) originating from the center of M87 is resolved at different wavelengths (radio, optical, and x-ray). The observed inclination of the jet, at an angle of $\sim 30^\circ$ relative to the observer’s line of sight (3), demonstrates that M87 is not a blazar and hence would represent a new class of TeV γ -ray emitters. M87 has also been suggested as an accelerator of the enigmatic ultra-high-energy (10^{20} eV) cosmic rays (4, 5). Previously, weak evidence for $E > 730$ GeV γ -ray emission from M87 in 1998 and 1999 with a statistical significance of 4.1 SDs was reported

by the High Energy Gamma Ray Astronomy (HEGRA) collaboration (6). No emission above 400 GeV was observed by the Whipple collaboration (7) from 2000–2003.

The observations reported here were performed with the High Energy Stereoscopic System (H.E.S.S.) located in Namibia. H.E.S.S. is an array of four imaging atmospheric-Cherenkov telescopes used for the measurement of cosmic γ rays of energies between 100 GeV and several 10 TeV [see (8) for more details]. The observations of M87 were performed between 2003 and 2006, yielding a total of 89 hours of data after quality selection cuts. After calibration (9), the H.E.S.S. standard analysis was applied to the data using hard event selection cuts (10). More information about the standard analysis, as well as a more recent, alternative analysis technique (11) which gives consistent results, can be found in (12).

An excess of 243 γ -ray events is measured from the direction of M87 in the whole data set, corresponding to a statistical significance of 13 SDs, establishing M87 as a TeV γ -ray source (Fig. 1). The position of the excess (right ascension, α ; declination, δ) was found to be $\alpha = 12^{\text{h}}30^{\text{m}}47.2^{\text{s}} \pm 1.4^{\text{s}}$, $\delta = +12^\circ23'51'' \pm 19''$

(J2000.0). This is, within the quoted statistical error and the systematic pointing uncertainty of the H.E.S.S. telescopes ($\sim 20''$ in both the right ascension and declination directions) compatible with the nominal (radio) position (13) of the nucleus of M87 ($\alpha = 12^{\text{h}}30^{\text{m}}49.4^{\text{s}}$, $\delta = +12^\circ23'28''$). Considering the angular resolution of H.E.S.S., the source is consistent with a pointlike object with an upper limit for a Gaussian surface-brightness profile of 3 arc min (99.9% confidence level). At the distance of M87 (16 Mpc), this corresponds to a radial extension of 13.7 kpc, which can be compared with the large-scale structure of M87 as seen at radio wavelengths (Fig. 1). A constraint on the size of the TeV emission region that is $\sim 10^6$ times as strong is deduced from the observed short-term flux variability, as shown below.

The differential energy spectra obtained for the 2004 and 2005 data sets (Fig. 2) are both well fit by a power-law function $dN/dE \propto E^{-\Gamma}$. The spectrum measured in 2005 is found to be hard ($\Gamma \sim 2.2$) and reaches beyond 10 TeV, with

¹Max-Planck-Institut für Kernphysik, Post Office Box 103980, D 69029 Heidelberg, Germany. ²Yerevan Physics Institute, 2 Alikhanian Brothers Street, 375036 Yerevan, Armenia. ³Centre d’Etude Spatiale des Rayonnements, CNRS/UPS, 9 avenue du Colonel Roche, BP 4346, F-31029 Toulouse Cedex 4, France. ⁴Universität Hamburg, Institut für Experimentalphysik, Luruper Chaussee 149, D 22761 Hamburg, Germany. ⁵Institut für Physik, Humboldt-Universität zu Berlin, Newtonstrasse 15, D 12489 Berlin, Germany. ⁶Laboratoire Univers et Théories, UMR 8102 du CNRS, Observatoire de Paris, Section de Meudon, F-92195 Meudon Cedex, France. ⁷University of Durham, Department of Physics, South Road, Durham DH1 3LE, UK. ⁸Unit for Space Physics, North-West University, Potchefstroom 2520, South Africa. ⁹Laboratoire Leprince-Ringuet, IN2P3/CNRS, Ecole Polytechnique, F-91128 Palaiseau, France. ¹⁰Laboratoire d’Annecy-le-Vieux de Physique des Particules, IN2P3/CNRS, 9 Chemin de Bellevue, BP 110 F-74941 Annecy-le-Vieux Cedex, France. ¹¹Astro Particule et Cosmologie, UMR 7164 (Université Paris 7, CNRS, CEA, Observatoire de Paris), 10 rue Alice Domon et Léonie Duquet, 75025 Paris Cedex 13, France. ¹²Dublin Institute for Advanced Studies, 5 Merrion Square, Dublin 2, Ireland. ¹³Landessternwarte, Universität Heidelberg, Königstuhl, D 69117 Heidelberg, Germany. ¹⁴Laboratoire de Physique Théorique et Astroparticules, IN2P3/CNRS, Université Montpellier II, CC 70, Place Eugène Bataillon, F-34095 Montpellier Cedex 5, France. ¹⁵DAPNIA/DSM/CEA, CE Saclay, F-91191 Gif-sur-Yvette Cedex, France. ¹⁶Laboratoire d’Astrophysique de Grenoble, Institut National des Sciences de l’Univers/CNRS, Université Joseph Fourier, BP 53, F-38041 Grenoble Cedex 9, France. ¹⁷Institut für Astronomie und Astrophysik, Universität Tübingen, Sand 1, D 72076 Tübingen, Germany. ¹⁸Laboratoire de Physique Nucléaire et de Hautes Energies, IN2P3/CNRS, Universités Paris VI and VII, 4 Place Jussieu, F-75252 Paris Cedex 5, France. ¹⁹Institute of Particle and Nuclear Physics, Charles University, V Holesovickach 2, 180 00 Prague 8, Czech Republic. ²⁰Institut für Theoretische Physik, Lehrstuhl IV, Weltraum und Astrophysik, Ruhr-Universität Bochum, D 44780 Bochum, Germany. ²¹University of Namibia, Private Bag 13301, Windhoek, Namibia. ²²Universität Erlangen-Nürnberg, Physikalisches Institut, Erwin-Rommel-Str. 1, D 91058 Erlangen, Germany. ²³European Associated Laboratory for Gamma-Ray Astronomy, jointly supported by CNRS and Max-Planck-Gesellschaft.

*To whom correspondence should be addressed. E-mail: matthias.beilicke@desy.de

†Present address: Purdue University, Department of Physics, 525 Northwestern Avenue, West Lafayette, IN 47907–2036, USA.

an average γ -ray flux of a factor of ~ 5 as high as in 2004.

The total γ -ray flux above 730 GeV (Fig. 3) for the individual years from 2003 to 2006 indicates variability on a yearly basis (14) corresponding to a statistical significance of 3.2 SDs, being derived from a χ^2 fit of a constant function. The variability is confirmed by a Kolmogorov test comparing the distribution of photon arrival times to the distribution of background arrival times, yielding a statistical significance for burst-like (nonconstant) behavior of the source of 4.5 SDs. Unexpectedly, variability on time scales of days (flux doubling) was found in the high-state data of 2005 (Fig. 3A), with a statistical significance of more than 4 SDs. This is the fastest variability observed in any wave band from M87 and strongly constrains the size of the emission region of the TeV γ radiation, which is further discussed below. No indications for short-term variability were found in the data of 2003, 2004, and 2006, which is not unexpected given the generally lower statistical significances of the γ -ray excesses in those years.

These observational results (location, spectrum, and variability) challenge most scenarios of very-high-energy γ -ray production in extragalactic sources. Although the luminosity ($\approx 3 \times 10^{40}$ erg/s) of TeV γ rays is quite modest and does not cause any problems with the global energy budget of the active galaxy M87, several models can be dismissed. The upper limit on the

angular size of ~ 3 arc min (13.7 kpc $\approx 4.3 \times 10^{22}$ cm) centered on the M87 nucleus position already excludes the core of the Virgo cluster (15) and outer radio regions of M87 as TeV γ -ray emitting zones. Further, the observed variability on time scales of $\Delta t \sim 2$ days requires a very compact emission region because of the light-crossing time. The characteristic size is limited to $R \leq c \times \Delta t \times \delta \approx 5 \times 10^{15} \delta$ cm $\approx 5 \times \delta R_s$, where δ is the relativistic Doppler factor (16) of the source of TeV radiation and $R_s \approx 10^{15}$ cm is the Schwarzschild radius of the M87 supermassive black hole. For any reasonable value of the Doppler factor (i.e., $1 < \delta < 50$, as used in the modeling of TeV γ -ray blazars), this implies a drastic constraint on the size of the TeV γ -ray source, which immediately excludes several potential sites and hypotheses of γ -ray production. First of all this concerns the elliptical galaxy M87 (15) and the γ -ray production due to dark matter annihilation (17). The most obvious candidate for efficient particle acceleration (18), namely the entire extended kiloparsec jet, is also excluded. Although compatible with the TeV source position, even the brightest knot in the jet (knot A) appears excluded, with its typical size on the order of one arc sec (about 80 pc $\approx 2.5 \times 10^{20}$ cm) resolved in the x-ray range (19).

An interesting possibility would be the peculiar knot (HST-1) in the jet of M87 (see supporting online text and fig. S2), a region of many violent events, with x-ray flares exceeding

the luminosity of the core emission (20) and superluminal blobs being detected downstream. Modeling the high-energy radiation properties of this region (by synchrotron and inverse-Compton scenarios), several authors favor sizes in the range of 0.1 to 1 pc (for moderate values of the Doppler factor ranging between 2 and 5) (20–22). Formally, though, there is no robust lower limit on the size of HST-1; therefore, we cannot exclude HST-1 as a source of TeV γ rays. However, it would be hard to realize the short-term variability of the TeV γ -ray emission in relation to HST-1, at least within the framework of current models. Because the size of the γ -ray production region does not exceed $R \leq 5 \times 10^{15} \delta$ cm, the location of HST-1 along the jet at 0.85 arc sec from the nucleus, which corresponds to $d \approx 65$ pc $\approx 2 \times 10^{20}$ cm, implies that the energy would be channeled from the central object into the γ -ray production region within an unrealistically small opening angle $\sim R/d \approx 1.5 \times 10^{-3} \delta$ degree.

The only remaining and promising possibility is to conclude that the site of TeV γ -ray production is the nucleus of M87 itself (23). In contrast to the established TeV γ -ray blazars, the large-scale jet of M87 is seen at a relatively large jet angle ($\theta \sim 30^\circ$), which suggests a quite modest Doppler boosting of its radiation. Nevertheless, because of the proximity of M87, both leptonic (24) and hadronic (5, 25) models predicted detectable TeV γ -ray emission. How-

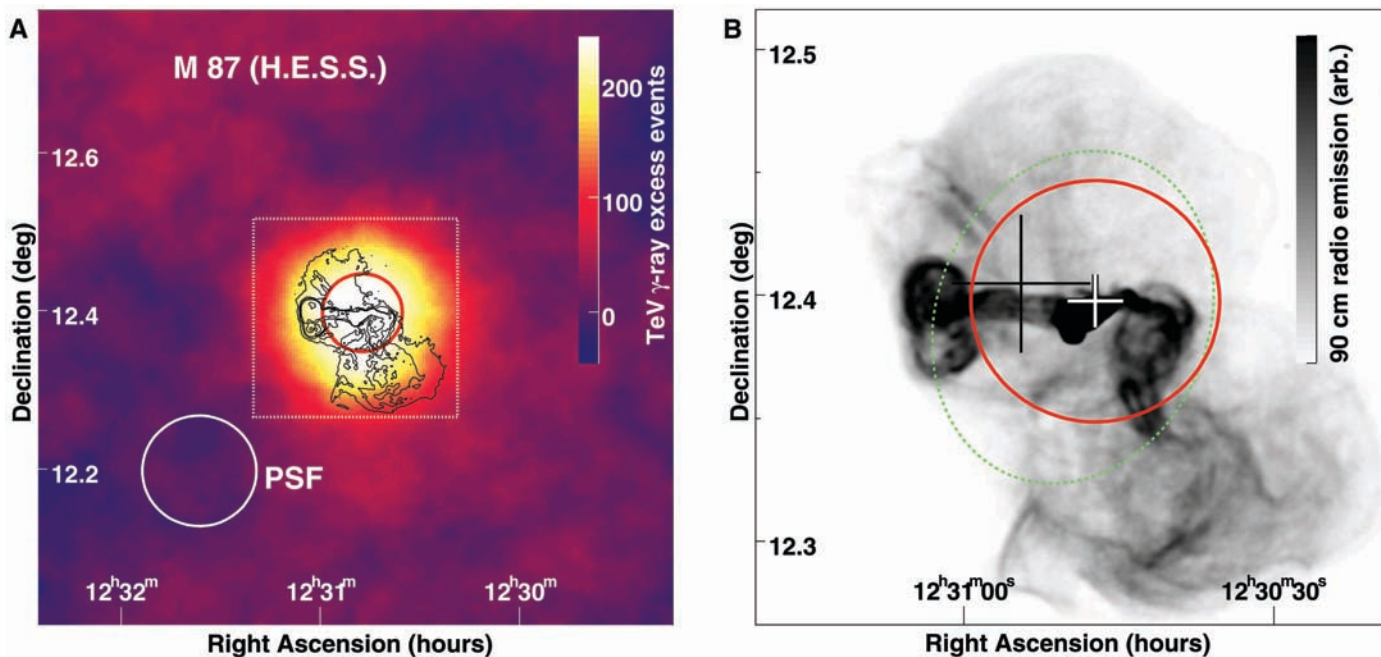


Fig. 1. Shown are the sky map as well as the position and extension limit of the TeV γ -ray emission from M87. **(A)** Smoothed TeV γ -ray excess map (color coded, 0.1° integration radius) as measured by H.E.S.S. The size (68% containment radius) of the H.E.S.S. point-spread function (PSF) is also indicated. The red circle indicates the intrinsic extension upper limit (99.9% confidence level) of 3 arc min of the TeV γ -ray excess corresponding to 13.7 kpc in M87. The contour lines show the 90-cm radio emission (32). The white box marks the cutout shown in **(B)**. **(B)** The 90-cm

radio data (32) measured with the Very Large Array, together with the TeV position with statistical and $20''$ pointing uncertainty errors (white cross) and again the 99.9% confidence level extension upper limit (red circle). The size of the emission region deduced from the short-term variability is smaller by a factor of $\sim 10^6$. The black cross marks the position and statistical error of the γ -ray source reported by HEGRA. The green ellipse indicates the host galaxy seen in the optical wavelengths with an extension of 8.3×6.6 arc min in diameter.

ever, these scenarios typically produce a soft energy spectrum of TeV γ rays, clearly in contrast to the hard spectrum measured by H.E.S.S. Leptonic models can be adapted in various ways to match the new results. Within synchrotron self-Compton (SSC) scenarios (26), one method is to consider the possibility of differential Doppler-boosting in the jet near the core region, a phenomenon clearly expected in the jet formation zone, which extends over <0.1 pc from the nucleus (27). Emitting plasma blobs of small sizes with Doppler factors between 5 and 30 and magnetic fields well below equipartition can account for the observed TeV γ -ray emission. An additional flux contribution from inverse-Compton scattering of background photons, coming from scattered disk emission or from dust, can further reduce the range of Doppler factors toward moderate values.

The TeV γ -ray photons (independent of their production mechanism) might be absorbed by the pair-absorption process $\gamma_{\text{TeV}} + \gamma_{\text{IR}} \rightarrow e^+ e^-$ on the local infrared (IR) radiation field in the TeV γ -ray emission region. Because no signature for an absorption can be identified in the energy spectrum up to 10 TeV, one can derive an upper limit on the luminosity of the infrared radiation field at 0.1 eV (corresponding to a wavelength of ~ 10 μm , most relevant for absorption of 10 TeV γ rays) to be $L(0.1 \text{ eV}) \leq 3.6 \times 10^{38} (R/10^{15} \text{ cm}) \text{ erg/s}$, where R is the size of the TeV γ -ray emission region. Such a low central

IR radiation luminosity supports the hypothesis of an advection-dominated accretion disk (i.e., an accretion disk with low radiative efficiency) in M87 (28) and generally excludes a strong contribution of external inverse-Compton emission on IR light to the TeV γ -ray flux.

If one accepts the hypothesis that protons can be accelerated as high as 10^{20} eV in jets of radio galaxies, then (hadronic) proton synchrotron models (5, 25) cannot be excluded, considering the presented data. An alternative γ -ray production mechanism is curvature radiation of ultra-high-energy protons in the immediate vicinity of the supermassive black hole. This novel mechanism can simultaneously explain both the hard spectrum and fast variability of the observed TeV γ -ray emission. Rapidly rotating black holes embedded in externally supported magnetic fields can generate electric fields and accelerate protons to energies up to 10^{20} eV (29–31). Assuming that acceleration of protons takes place effectively within 3 Schwarzschild radii R_s , and if the horizon threading magnetic field is not much below 10^4 G, one should expect γ -ray radiation due to proton curvature radiation extending to at least 10 TeV. (The electron curvature radiation is less likely because of severe energy losses even in a tiny

component of an irregular magnetic field.) No correlation with fluxes at other wavelengths is expected in this model. Although the size of the γ -ray production region, $R \sim 3 R_s \sim 3 \times 10^{15}$ cm, perfectly matches the observed variability scale, and the model allows extension of the γ -ray spectrum to 10 TeV without any significant correlation at other wavelengths, the main problem of the model is the suggested magnetic field. It is orders of magnitude larger than the B field expected from the accretion process, given the very low accretion rate as it follows from the bolometric luminosity of the core as well as the estimates of the power of the jet in M87.

The time scale of the short-term variability of the TeV γ rays is on the order of the light-crossing time of the black hole (located at the center of M87), which is a natural time scale of the object. Therefore, the results reported here give clear evidence for the production of TeV γ rays in the immediate vicinity of the black hole of M87.

References and Notes

1. F. Macchetto *et al.*, *Astrophys. J.* **489**, 579 (1997).
2. H. L. Marshall *et al.*, *Astrophys. J.* **564**, 683 (2002).

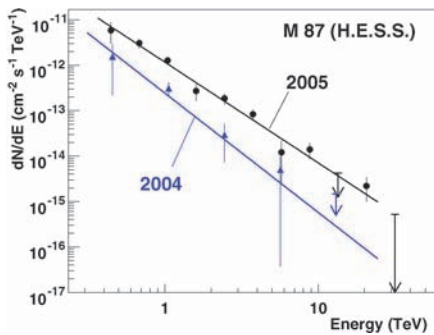


Fig. 2. The differential energy spectrum of M87 obtained from the 2004 and the 2005 data [using standard event selection cuts (10)], covering a range of ~ 400 GeV to ~ 10 TeV. Spectra for the 2003 and 2006 data sets could not be derived because of limited event statistics. Flux points with a statistical significance less than 1.5 SDs are given as upper limits (99.9% confidence level). The corresponding fits of a power-law function $dN/dE = I_0 \times (E/1 \text{ TeV})^{-\Gamma}$ are indicated as lines. The photon indices are $\Gamma = 2.62 \pm 0.35$ (2004 data) and $\Gamma = 2.22 \pm 0.15$ (2005 data). Aside from the difference in the flux normalization by a factor of ~ 5 [$I_0 = (2.43 \pm 0.75) \times 10^{-13} \text{ cm}^{-2} \text{ s}^{-1} \text{ TeV}^{-1}$ in 2004 and $I_0 = (11.7 \pm 1.6) \times 10^{-13} \text{ cm}^{-2} \text{ s}^{-1} \text{ TeV}^{-1}$ in 2005], no variation in spectral shape is found within errors. The systematic error on the photon index and flux normalization are estimated to be $\Delta\Gamma = 0.1$ and $\Delta I_0/I_0 = 0.2$, respectively.

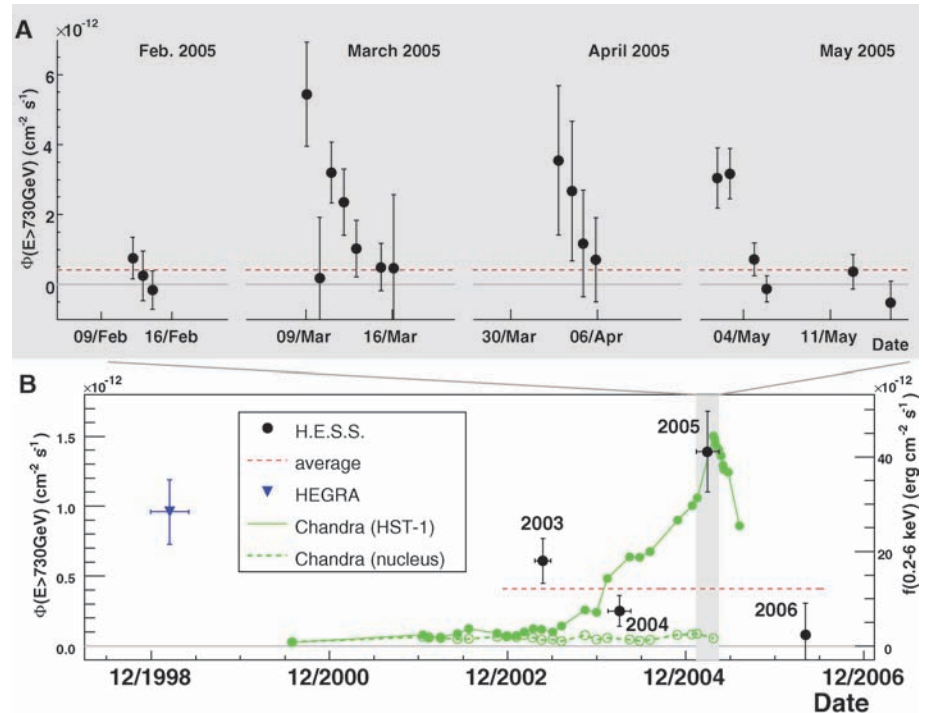


Fig. 3. Gamma-ray flux above an energy of 730 GeV as a function of time. The given error bars correspond to 1 SD statistical errors. (B) The average flux values for the years 2003 to 2006 as measured with H.E.S.S., together with a fit of a constant function (red line). The flux reported by HEGRA is also drawn (a systematic error must be taken into account when comparing results from the two instruments). (A) The night-by-night fluxes for the four individual months (February to May) of the high-state measurements in 2005, with significant variability on (flux doubling) time scales of ~ 2 days. The green points in (B) correspond to the 0.2 – 6 keV x-ray flux of the knot HST-1 [solid, (20)] and the nucleus [dashed, (33)] as measured by Chandra; the lines are linear interpolations of the flux points. No unambiguous correlation between the flux of x rays and TeV γ rays can be identified (the x-ray/TeV data were not gathered simultaneously).

3. G. V. Bicknell, M. C. Begelman, *Astrophys. J.* **467**, 597 (1996).
4. P. L. Biermann *et al.*, *Nucl. Phys. B Proc. Suppl.* **87**, 417 (2000).
5. R. J. Protheroe *et al.*, *Astropart. Phys.* **19**, 559 (2003).
6. F. Aharonian *et al.*, HEGRA collaboration, *Astron. Astrophys.* **403**, L1 (2003).
7. S. Le Bohec *et al.*, *Astrophys. J.* **610**, 156 (2004).
8. W. Hofmann, *Proc. 29th Int. Cosmic Ray Conf. (Pune)*, **10**, 97 (2005).
9. F. Aharonian *et al.*, H.E.S.S. collaboration, *Astropart. Phys.* **22**, 109 (2004).
10. W. Benbow, *Proceedings: Towards a Network of Atmospheric Cherenkov Detectors VII (Palaiseau)*, 163 (2005).
11. M. de Naurois, *Proceedings: Towards a Network of Atmospheric Cherenkov Detectors VII (Palaiseau)*, 149 (2005); <http://arxiv.org/abs/astro-ph/0607247>.
12. Materials and methods are available as supporting online material on Science Online.
13. C. Ma *et al.*, *Astronom. J.* **116**, 516 (1998).
14. M. Beilicke *et al.*, *Proc. of TEXAS Symposium on Relativistic Astrophysics* (Stanford University), Paper #2403 (2004), see <http://arxiv.org/abs/astro-ph/0504395>.
15. C. Pfommer, T. A. Enßlin, *Astron. Astrophys.* **407**, L73 (2003).
16. Emission from a region that is moving with a relativistic speed $\beta = v/c$ (c is the speed of light) is boosted along the direction of movement (relativistic beaming). The boost is a function of the observation angle θ relative to this direction and is described by the Doppler factor $\delta = [\Gamma(1 - \beta \cos \theta)]^{-1}$, where $\Gamma = (1 - \beta^2)^{-1/2}$ is the Lorentz factor of the emission region.
17. E. A. Baltz *et al.*, *Phys. Rev. D* **61**, 3514 (2000).
18. L. Stawarz *et al.*, *Astrophys. J.* **626**, 120 (2005).
19. E. S. Perlman, A. S. Wilson, *Astrophys. J.* **627**, 140 (2005).
20. D. E. Harris *et al.*, *Astrophys. J.* **640**, 211 (2006).
21. D. E. Harris *et al.*, *Astrophys. J.* **586**, L41 (2003).
22. L. Stawarz *et al.*, *Mon. Not. R. Astron. Soc.* **370**, 981 (2006).
23. W. Forman *et al.*, *Astrophys. J.* **635**, 894 (2005).
24. M. Georganopoulos *et al.*, *Astrophys. J.* **634**, L33 (2005).
25. A. Reimer *et al.*, *Astron. Astrophys.* **419**, 89 (2004).
26. D. L. Band, J. E. Grindlay, *Astrophys. J.* **308**, 576 (1986).
27. W. Junor, J. A. Biretta, M. Livio, *Nature* **401**, 891 (1999).
28. C. S. Reynolds, T. di Matteo, A. C. Fabian, U. Hwang, C. R. Canizares, *Mon. Not. R. Astron. Soc.* **283**, L111 (1996).
29. A. Levinson, *Phys. Rev. Lett.* **85**, 912 (2000).
30. E. Boldt, M. Loewenstein, *Mon. Not. R. Astron. Soc.* **316**, 29 (2000).
31. F. A. Aharonian, A. A. Belyanin, E. V. Derishev, V. V. Kocharovskiy, V. V. Kocharovskiy, *Phys. Rev. D* **66**, 023005 (2002).
32. F. N. Owen *et al.*, *Proceedings of The Universe at Low Radio Frequencies, ASP Conf. Ser.*, 199 (2000); <http://xxx.lanl.gov/abs/astro-ph/0006152>.
33. Provided by D. Harris, private communication.
34. The support of the Namibian authorities and of the University of Namibia in facilitating the construction and operation of H.E.S.S. is gratefully acknowledged, as is the support by the German Ministry for Education and Research (BMBF), the Max Planck Society, the French Ministry for Research, the CNRS-IN2P3, and the Astroparticle Interdisciplinary Programme of the CNRS, the UK Particle Physics and Astronomy Research Council (PPARC), the Institute of Particle and Nuclear Physics of the Charles University, the South African Department of Science and Technology and National Research Foundation, and the University of Namibia. We thank D. Harris for providing the Chandra x-ray light curve of the M87 nucleus.

Supporting Online Material

www.sciencemag.org/cgi/content/full/1134408/DC1

Materials and Methods

SOM Text

Figs. S1 and S2

Table S1

References

28 August 2006; accepted 11 October 2006

Published online 26 October 2006;

10.1126/science.1134408

Include this information when citing this paper.

Solid-State Qubits with Current-Controlled Coupling

T. Hime,¹ P. A. Reichardt,¹ B. L. T. Plourde,^{1,2} T. L. Robertson,^{1*} C.-E. Wu,^{1†}
A. V. Ustinov,^{1‡} John Clarke^{1§}

The ability to switch the coupling between quantum bits (qubits) on and off is essential for implementing many quantum-computing algorithms. We demonstrated such control with two flux qubits coupled together through their mutual inductances and through the dc superconducting quantum interference device (SQUID) that reads out their magnetic flux states. A bias current applied to the SQUID in the zero-voltage state induced a change in the dynamic inductance, reducing the coupling energy controllably to zero and reversing its sign.

The past few years have seen major advances in the field of superconducting quantum bits (qubits). This family includes those based on electrical charge (1), magnetic flux (2–4), charge and phase (5), and the phase difference across a Josephson junction (6). Arbitrary superpositions of the single-qubit states can be prepared and manipulated by microwaves to produce Rabi oscillations, Ramsey fringes, and echoes long-familiar in atomic physics and nuclear magnetic resonance (7). The

prepared quantum states remain coherent for times up to several microseconds (8). Coupling two or more qubits together results in entangled states (9–15) with energy spectra that exhibit the avoided crossings (anticrossings) predicted by quantum mechanics (16). In addition to studying quantum coherence in many-body systems, there is considerable interest in arrays of qubits for quantum computing. Because quantum computation requires both the manipulation of single qubits and the entanglement of many qubits, the ability to switch the coupling (17–21) between qubits on and off in a scalable architecture would enable many quantum-computing algorithms.

We conducted experiments on two flux qubits biased at the same frequency. In this regime, the antiferromagnetic interaction between the qubits produces an anticrossing and thus a splitting in the energy spectrum of the first and second excited states. By varying the bias current in the zero-voltage state of the superconducting quantum interference device (SQUID) used

to read out the flux states of the coupled qubits, we reduced the coupling energy and hence the splitting of the two energy levels of the excited states to zero. Indeed, as predicted, we can even change the interaction from antiferromagnetic to ferromagnetic. Furthermore, we showed that the transition probability from the symmetric ground state to an antisymmetric excited state vanishes at the anticrossing, in qualitative agreement with calculations.

Each flux qubit consists of a superconducting loop interrupted by three Josephson tunnel junctions (2). When the applied magnetic flux Φ_q is at the degeneracy point $(n + 1/2)\Phi_0$ (where n is an integer such that $|\Phi_q - n\Phi_0| \leq \Phi_0/2$, $\Phi_0 \equiv h/2e$ is the flux quantum, h is the Planck constant, and e is the electron charge), a screening current I_q can flow around the loop in either direction, represented by the states $|\uparrow\rangle$ and $|\downarrow\rangle$. The ground and first excited states of the qubit correspond to symmetric and antisymmetric superpositions of the two current states and are separated by an energy Δ . When $\Phi_q \neq (n + 1/2)\Phi_0$, the energy difference increases to $v = (\Delta^2 + \varepsilon^2)^{1/2}$, where $\varepsilon = 2I_q[\Phi_q - (n + 1/2)\Phi_0]$. The state of the qubit is measured by coupling the flux generated by I_q to a dc SQUID. Two flux qubits are coupled through their mutual inductances to each other and to the SQUID. The interaction of two pairs of states produces four new states: a ground state $|0\rangle$ and three excited states $|1\rangle$, $|2\rangle$, and $|3\rangle$. Each of these states consists of a linear superposition of four basis states (22): the symmetric triplet $|\uparrow\uparrow\rangle$, $|S\rangle = (|\uparrow\downarrow\rangle + |\downarrow\uparrow\rangle)/2^{1/2}$, and $|\downarrow\downarrow\rangle$ and the antisymmetric singlet $|A\rangle = (|\uparrow\downarrow\rangle - |\downarrow\uparrow\rangle)/2^{1/2}$.

The two qubits A and B and their readout dc SQUID are shown schematically in Fig. 1A. The qubits have loop inductances L_{qA} and L_{qB} and

¹Department of Physics, University of California, Berkeley, CA 94720–7300, USA. ²Department of Physics, Syracuse University, Syracuse, NY 13244–1130, USA.

*Present address: Proteus Biomedical, 750 Chesapeake Drive, Redwood City, CA 94063, USA.

†Present address: Department of Physics, National Tsing-hua University, Hsinchu 300, Taiwan.

‡Permanent address: Physikalisches Institut III, Universität Erlangen-Nürnberg, Erwin-Rommel-Strasse 1, D-91058 Erlangen, Germany.

§To whom correspondence should be addressed. E-mail: jclarke@berkeley.edu